51st AIAA Aerospace Sciences Meeting including the New Horizons Forum and Aerospace Exposition
07 - 10 January 2013, Grapevine (Dallas/Ft. Worth Region), Texas

AIAA 2013-1172

Purely Gasdynamic Multidimensional Indirect Detonation Initiation Using Localized Acoustic Timescale Power Deposition

J. D. Regele*
Iowa State University, Ames, IA, 50011, USA
D. R. Kassoy,† A. Vezolainen and O. V. Vasilyev‡
University of Colorado, Boulder, CO 80309, USA

A "purely gasdynamic" indirect detonation initiation process is presented that can be independent of diffusion, viscosity and turbulence, and does not require direct initiation. In this process, energy is deposited into a finite volume of fluid in an amount of time that is similar to the acoustic timescale of the fluid volume. Highly resolved two-dimensional simulations show that the artificial diffusion implicit in the numerical method is demonstrated to accelerate detonation formation. It is shown that given sufficient resolution, the detonation formation time becomes dependent only on large-scale gasdynamics and is independent of the small scale structures.

I. Introduction

Traditionally, combustion modelers have concluded that detonations form either by direct initiation or by Deflagration-to-Detonation Transition (DDT). Direct initiation uses a large amount of energy deposited in a short time period such that a blast wave is created inside the reactive gas mixture. A typical DDT process begins by igniting the gas using a small amount of energy to create a laminar flame deflagration. Surface instabilities at the flame front transform the deflagration to a turbulent reaction front. Compression waves are produced from the enhanced rate of energy release from the increase in flame surface area, which preheat the reactive gas ahead of the reaction front until a detonation wave is formed. Diffusion, viscosity, and turbulence play a major role in detonations and DDT alike .[1,2,3,4,5]

Direct initiation and DDT can be seen as two limiting extremes on a continuum scale using the acoustic timescale theory of Kassoy.[6] Consider a fluid volume of length scale l and sound speed a such that the acoustic timescale of the fluid volume can be defined $t_a = l/a$. If heat is added to the fluid volume on a timescale t_h that is short compared to the acoustic timescale $t_h \ll t_a$ then the fluid experiences nearly constant volume heat addition. The amount of energy added to the volume determines whether it will form acoustic, shock, or blast waves. In the event of blast wave formation, this limit corresponds roughly to the direct initiation process. On the opposite extreme, if $t_h \gg t_a$ then a spatially homogeneous pressure transient arises from the slower heat addition. A detonation is then formed through a typical DDT process.[7]

The focus of the current work is on acoustic timescale detonation initiation, where the heat is deposited on a timescale similar to the acoustic timescale $t_h \sim t_a$. Previous work in this area has focused on 1-D simulations of the reactive Euler equations.[8,9,10,11] The simulations begin with a reactive mixture initially at rest and spatially resolved thermal power addition is imparted to the fluid over a timescale $t_h \sim t_a$. Shock waves are created from the initial power deposition, but unlike direct detonation initiation, the reaction front becomes fully decoupled from the initial shock wave. Hot spots are formed which eventually react on a timescale short compared to the acoustic timescale leading to the subsequent formation of a detonation. The studies originally focused on relatively low activation energies with heat conducted through a wall.[8,9] Heat

*Assistant Professor of Aerospace Engineering, Iowa State University, AIAA member, jregele@iastate.edu.
†Professor Emeritus of Mechanical Engineering, University of Colorado, AIAA member.
‡Professor of Mechanical Engineering, University of Colorado, AIAA member.

was later added directly to a fluid volume.[10] Recently the work was extended to higher activation energies[11] and demonstrated a multiple hot-spot behavior typical of high activation energy mixtures.

The objective of the current work is to extend the acoustic timescale approach to two dimensions. Since heat release on the acoustic timescale is the defining feature of this work, it is desirable to continue the investigation using "purely gasdynamic" heating. Thus, the current work seeks an indirect detonation initiation process that is essentially independent of diffusional transport effects.

Before embarking on such an effort, it is advantageous to determine if it is reasonable to assume such a behavior will be possible. When performing DDT simulations, the Navier-Stokes equations are normally solved because molecular viscosity/diffusion effects are known to play a major role in DDT .[12,13,14,15,1,16,17] In the instances where the Euler equations are solved without the diffusive/viscous terms, the numerical diffusion implicitly present in the hyperbolic solver is used to mimic the effects of molecular viscosity/diffusion.[18]

Within the context of resolving detonation structure, there is currently much debate[2,4,5] over molecular diffusion, numerical diffusion, when it is valid to use the Euler equations, and when it is better to use the Navier-Stokes equations. In regular detonations, shock compression is sufficient to react all the fluid that passes through the shock front, which creates a regular spacing of transverse waves with little evidence of turbulence behind the initial shock front. Unstable detonations are characterized by irregular transverse wave spacing and a high level of turbulence located behind the initial shock front. It has been shown for very regular detonations that there is little difference between Euler and Navier-Stokes solutions.[19] However, unstable detonations form unreacted pockets that propagate downstream. In these cases, it has been shown that in order to be quantitatively accurate, the diffusive and viscous transport effects should be included.[2,4] It was shown in Ref. 2 that for mildly unstable detonations it is possible to accurately resolve the consumption time of unreacted pockets that travel relatively small distances into the burned gases. However, for highly unstable detonations where the unreacted pockets penetrate deep inside the reacted gases, turbulent mixing and diffusion are found to play a major role in enhancing the burning rate of these pockets.[4]

The Richtmyer-Meshkov instability is found to be the primary source of turbulence generation in DDT.[1,15] Kelvin-Helmholtz instabilities can also be found in DDT as a secondary instability and are often suppressed by diffusive effects in Navier-Stokes solutions.[1]

In order to obtain a "purely gasdynamic" indirect detonation initiation solution, it will be necessary to capture both the Richmyer-Meshkov and Kelvin-Helmholtz instabilities. It will also be necessary to minimize the diffusion such that any unreacted pockets that may form will have a minimal amount of heat diffused into them so that their autoignition times can be resolved. A moderately low activation energy will be used that is similar to that of the mildly unstable detonation case in Ref. 2. By using this activation energy, it will be possible to resolve the autoignition time of the unreacted pockets. The approach taken in this work to achieve these objectives is to solve the Euler equations and increase the resolution until the detonation formation time is no longer a function of resolution. Once this is achieved, the indirect detonation initiation process will be considered "purely gasdynamic".

II. Mathematical Model

Purely gasdynamic detonation initiation is modeled using the non-dimensional reactive Euler equations (see Table 1 for variable definitions). The governing equations for the conserved quantities density ρ, momentum $\rho\mathbf{u}$, total energy ρe_T and reactant density ρY are expressed as

$$\frac{\partial \rho}{\partial t} + \nabla \cdot \rho\mathbf{u} = 0, \tag{1a}$$

$$\frac{\partial \rho\mathbf{u}}{\partial t} + \nabla \cdot (\mathbf{u} \otimes \rho\mathbf{u}) + \nabla p = 0, \tag{1b}$$

$$\frac{\partial \rho e_T}{\partial t} + \nabla \cdot (\mathbf{u}(\rho e_T + p)) = \dot{Q}(\mathbf{x}, t) + \dot{W} q, \tag{1c}$$

$$\frac{\partial \rho Y}{\partial t} + \nabla \cdot \rho Y \mathbf{u} = -\dot{W}. \tag{1d}$$

An ideal gas equation of state and one-step Arrhenius reaction rate are defined

$$p = (\gamma - 1)\left(\rho e_T - \frac{1}{2}\rho u_{\mathrm{i}} u_{\mathrm{i}}\right), \tag{2}$$

$$\dot{W} = B\rho Y \exp(-E/T), \tag{3}$$

where q is the heat of reaction, Y is the reactant mass fraction and $\dot{Q}(\mathbf{x}, t)$ is an externally added power addition term. The Arrhenius reaction rate $\dot{W}$ is expressed in terms of the non-dimensional quantities. These include the pre-exponential factor B, the activation energy E, and the temperature $T = \gamma p/\rho$.

Table 1 defines the non-dimensional variables where the thermodynamic quantities (p, ρ, T) are expressed with respect to the undisturbed dimensioned (primed quantities) initial state (p'_o, ρ'_o, T'_o). The spatial vector $\mathbf{x}$ is defined with respect to a characteristic length l' in the undisturbed fluid such that the acoustic timescale $t'_a = l'/a'_o$, where ${a'}_o^2 = \gamma R' T'_o$.

Table 1. Non-dimensional variable definitions. Primes denote dimensional quantities.

Position	$\mathbf{x} = \mathbf{x}'/l'$
Time	$t = t'/t'_a$
Velocity	$\mathbf{u} = \mathbf{u}'/a'_o$
Pressure	$p = p'/\gamma p'_o$
Density	$\rho = \rho'/\rho'_o$
Temperature	$T = T'/T'_o$
Total Energy	$e_T = e'_T/{a'_o}^2$
Activation Energy	$E = E'/R'T'_o$
Heat of Reaction	$q = q'/{a'_o}^2$
External Power Deposition	$\dot{Q} = \dot{Q}' t'_a/\rho'_o {a'_o}^2$
Pre-exponential Factor	$B = B' t'_A$

III. Numerical Approach

Since the ultimate objective of this work is to obtain a "purely gasdynamic" indirect detonation initiation solution to the reactive Euler equations, a multiresolution hyperbolic solver is desired. In this study the dynamically Adaptive Wavelet-Collocation Method (AWCM) is used to perform the simulations.[20,21] The AWCM combines second generation wavelets with a prescribed error threshold parameter ϵ to determine which grid points are necessary in order to achieve a prescribed level of accuracy.

The hyperbolic solver developed for the AWCM is used to maintain numerical stability and reduce spurious oscillations across jump discontinuities.[22] As is common with all hyperbolic solvers, the method is first order accurate near shocks and contact discontinuities, and second order accurate in smooth regions. Other than the minimum grid spacing, the numerical diffusion/viscosity that is implicitly present in the solver is the primary source of grid dependence in the present work. A solution that is independent of diffusion/viscosity will be found by increasing the maximum level of resolution and thus decreasing the artificial diffusion/viscosity until it is determined to be independent of grid resolution. The numerical diffusion/viscosity essentially acts as a mechanism to demonstrate the transition between a detonation initiation process that is influenced by diffusion from a process that is relatively independent.

IV. Resolution Dependence in One Dimension

Before performing numerical simulations of "purely gasdynamic" acoustic timescale detonation initiation in two dimensions and analyzing the solution sensitivity to numerical resolution, it is helpful to first look at the numerical sensitivity of a previously performed one-dimensional simulation.[10,11] In this work, Case 1 in Ref. 11 is performed at multiple levels of resolution. The objective is to demonstrate that in one dimension the peak heat release time is relatively insensitive to grid spacing for a wide range of resolution.

The problem is solved using the 1-D reactive Euler Equations 1, the equation of state 2 and the Arrhenius reaction rate equation 3. Initially the reactive gas is at rest in thermal equilibrium with the initial condition

$$\rho_o = T_o = Y_o = 1 \qquad\qquad u_o = 0. \tag{4}$$

A spatially resolved, transient thermal power deposition

$$\dot{Q}(x,t) = \begin{cases} 0 & 0 \le x \le 1 \\ 3f(t)\cos\left[\frac{\pi}{4}(3-x)\right] & 1 < x \le 5 \\ 0 & x > 5 \end{cases} \tag{5}$$

$$f(t) = 0.7\Big(\tanh\Big[5\,(t-t_a)\Big] - \tanh\Big[5\,(t-t_b)\Big]\Big), \tag{6}$$

is deposited in the region $x \in [1,5]$ near the adiabatic reflecting wall located at $x = 0$. For this simulation the heat addition is limited within the times $t_a = 0.5$ and $t_b = 10$. The specific heat ratio $\gamma = 1.4$, heat of reaction $q = 15$, pre-exponential factor $B = 15$, and activation energy $E = 13.79$.

Four different simulations are performed using a base grid resolution $M_x = 200$. The effective grid resolution is specified in terms of the maximum level of resolution $j_{\max}$ such that the effective grid resolution $n_x = M_x \cdot 2^{j_{\max}}$. Effective grid resolutions n_x for the study range from 3200 to 51200 for $j_{\max} = 4$ to $j_{\max} = 8$.

Convergence comparisons are made using the globally integrated chemical heat release. The global heat release is defined as the integral over the fluid volume V of the chemical heat release rate at each instant in time so that

$$\dot{Q}_{ch}(t) = \int_V \dot{W}(t) q dV. \tag{7}$$

Figure 1 shows the globally integrated heat release as a function of different levels of resolution.

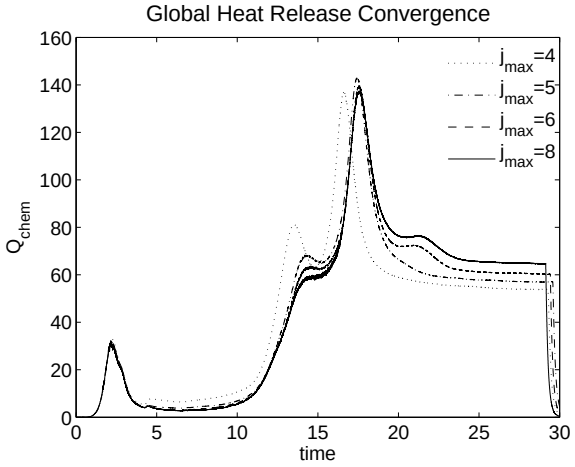

Figure 1. Global heat release curves are shown for varying levels of grid resolution. The peak heat release time varies by less than 6% for over the entire resolution range.

The results show that the peak heat release time in 1-D acoustic timescale DDT is a weak function of numerical resolution. At the minimum resolution $j_{\max} = 4$, the peak heat release time is within 5% of the converged value. The weak dependence of the peak heat release time on resolution is expected in one dimension. However, because of the hydrodynamic instabilities that form in multiple dimensions, it is anticipated that the resolution dependence will be stronger in the two-dimensional simulations.

V. Two-Dimensional Indirect Detonation Initiation

The one-dimensional model analyzed in the previous section can be extended to two dimensions by limiting the power deposition to a circular volume of fluid inside a rectangular domain. Simulations are performed at 5 different levels of resolution, where each increase in resolution effectively reduces the minimum grid spacing by one half.

V.A. Problem Statement

Each simulation begins with the reactive gas at rest with the initial condition

$$\rho_0 = p_0 = Y_0 = 1 \qquad\qquad \mathbf{v_0} = 0\,, \tag{8}$$

and transient thermal power deposition $\dot{Q}$ defined

$$\dot{Q}(\mathbf{x},t) = 4.2A\Big(\tanh\Big[5A\,(t-t_a)\Big] - \tanh\Big[5A\,(t-t_b)\Big]\Big)g(\mathbf{x}) \tag{9}$$

$$g(\mathbf{x}) = \begin{cases} 1 & \text{for } |\mathbf{x}| \le R \\ 0 & \text{for } |\mathbf{x}| > R\,. \end{cases} \tag{10}$$

The geometric term $g(\mathbf{x})$ limits the power addition to a circle of radius $R = 2$ centered at the origin. The power deposition lasts from t_a until $t_b = t_a + 9.5/A$, where A is the power deposition amplitude. The domain lies in $x \in [-3, 57]$ and $y \in [-3, 12]$ and reflecting slip walls are present on all walls except the exit $x = 57$. Each simulation uses a heat of reaction $q = 15$, specific heat ratio $\gamma = 1.4$, activation energy $E = 13.8$, and pre-exponential factor $B = 35$. Heat is added between $t_a = 0.5$ and $t_b = 5.25$ with $A = 2$.

The maximum level of resolution is varied from $5 \le j_{\max} \le 9$ with a base grid of 30×6. This corresponds to an effective grid of 15360×3072 for the $j_{\max} = 9$ case.

V.B. General Behavior

A sequence of temperature contours (Fig. 2) and the globally integrated heat release at each moment in time (Fig. 3) are used to illustrate the indirect detonation formation process. It takes approximately 24 acoustic time units for the over-driven detonation to form. Figure 2 shows a sequence of temperature contours for $2 \le t \le 24$ demonstrating the indirect detonation initiation process. Heat is deposited in a circle in the bottom left hand corner from $0.5 \le t \le 5.25$. The rapid deposition of heat creates compression waves that propagate away from the initially heated region. Figure 3 plots the globally integrated heat release (defined in eq. 7) as a function of time. Before $t = 2$, the reactants inside the deposition region are consumed in a chemical explosion, which adds additional heat to the deposition region. This heat release is seen as the first peak near $t = 2$ in Fig. 3. It is difficult to discern from the contour at $t = 2$, but the interface between the burning and reactive gas forms a rippled surface. It is thought that this is a result of the Darrieus-Landau instability at the burning gas interface because once the reactants are consumed the growth of surface fluctuations ceases.

At some point shortly after $t = 2$ when the compression waves first reflect off the left and bottom walls the compression waves become fully discontinuous shock waves. The reflected and transmitted shocks form Mach stems that propagate in the positive x- and y-directions. The reflected waves impinge on the burnt-unburnt gas interface and induce Richtmyer-Meshkov instabilities, which then increase the fluctuation magnitude at the material interface. This can be initially observed in the $t = 3.5$ contour.

At about $t = 2.5$, a second explosion occurs in the lower left corner when the shock waves reflect off the bottom and left walls and raise the pressure in that region in a duration short enough that the temperature rises with pressure. The reactive gas explodes once it has reached a sufficient temperature. This explosion consumes only a small amount of fluid, which makes the heat released barely visible in Fig. 3 at $t = 2.5$ shortly after the first peak at around $t = 2$.

In the $t = 5$ frame, the original outward propagating shock wave has reflected off the left and bottom walls and the Mach stems are clearly visible in the temperature contour. On the left wall, the leading edge of the shock wave is just about to reflect off the upper wall, starting in the upper left corner. When reflection occurs on the upper boundary, a hot spot appears in the upper left-hand corner of the channel, characterized by substantial local inertial confinement. This hot spot releases heat and generates compression waves that propagate away from the hot spot location. The heat released from this explosion corresponds to the peak in heat release rate shown in Fig. 3 at $t = 7.6$.

At $t = 7$, Fig. 2 shows the reflected wave re-enters the reacted region and is refracted, which induces an additional longitudinal component to the wave direction. Obviously, the creation of additional longitudinal compression waves through transverse wave refraction inside the reacted fluid medium is a mechanism not present in the previous 1-D work.[10,11,23] The transverse waves compress and heat previously unreacted fuel

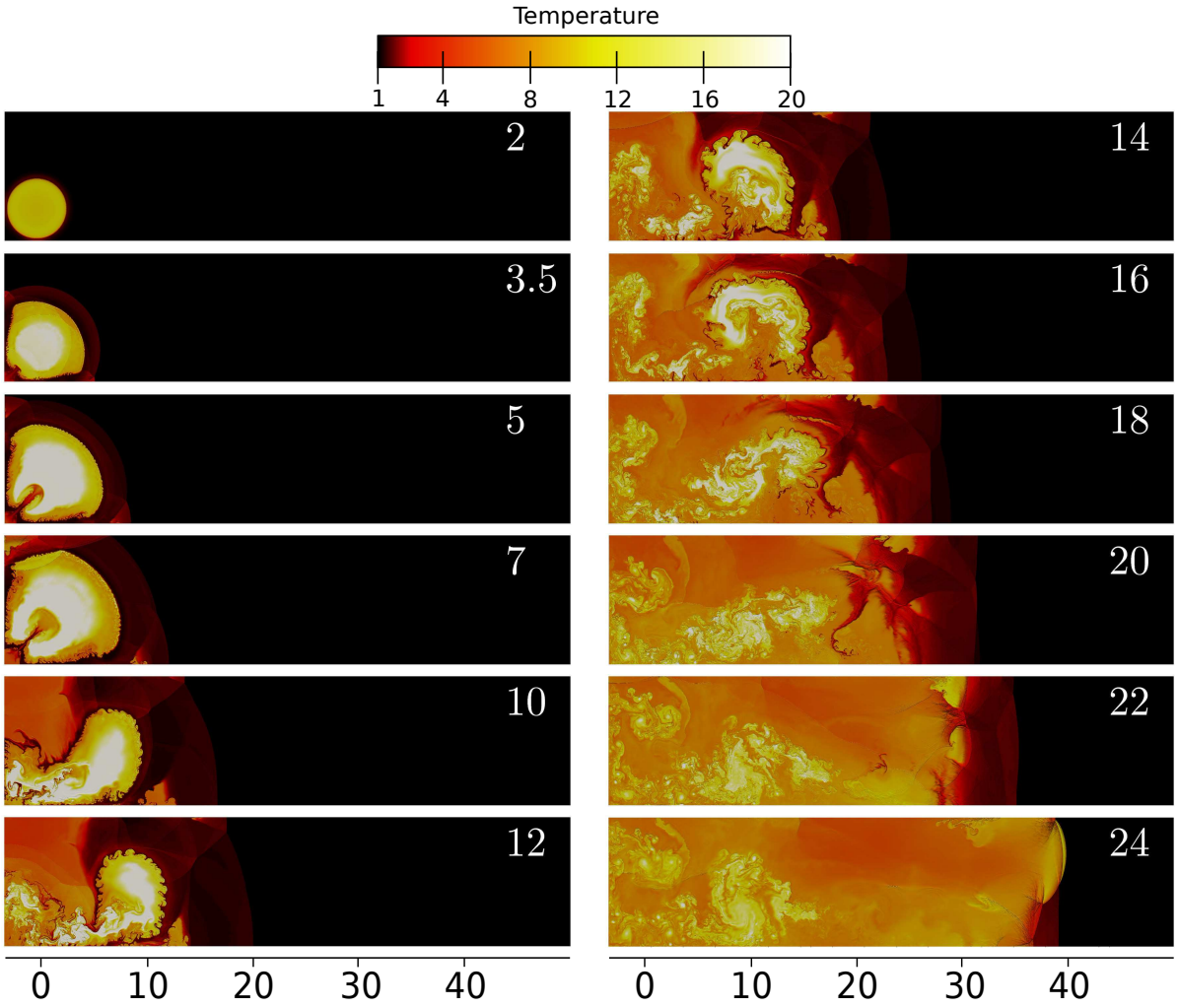

Figure 2. Sequence of temperature contours demonstrate the multidimensional indirect detonation formation process for $j_{\max} = 9$ at times $t = [2, 3.5, 5, 7, 10, 12, 14, 16, 18, 20, 22, 24]$.

pockets, which ignite and help produce additional longitudinal waves, as well as sustaining the transverse waves the reverberate off the top and bottom walls.

Kelvin-Helmholtz roll-up instabilities are clearly visible in frames $t = [10, 12, 14]$ at the burnt-unburnt gas interface with a fairly high level of detail. The existence of such a detailed interface serves as an indicator that any numerical diffusion present in the algorithm has been minimized to the point that these features are possible to capture.

Figure 3 shows that starting at about $t = 14$ the global heat release rate begins to grow and reaches a peak at approximately $t = 24$. This acceleration in heat release can be observed in the temperature contour sequence as the rapid consumption of fuel starting at $t = 14$ and ending at $t = 24$ with the formation of the over-driven detonation wave emerging from the lead shock front.

V.C. Resolution Dependence

As stated in the introduction, the approach used in this work to obtain a "purely gasdynamic" indirect detonation initiation is to increase the maximum level of resolution until it appears that the initiation process has become independent of the resolution and fine scale structures. Since the Euler equations are solved, there is no predefined length scale to resolve and the fine scale structure detail should increase indefinitely. However, a length or time scale is essentially introduced through the reaction source term, which suggests that some form of convergence may be possible. However, since the scale is introduced through a reaction source term without any diffusion defined scales, strong dependence on numerical resolution is anticipated.

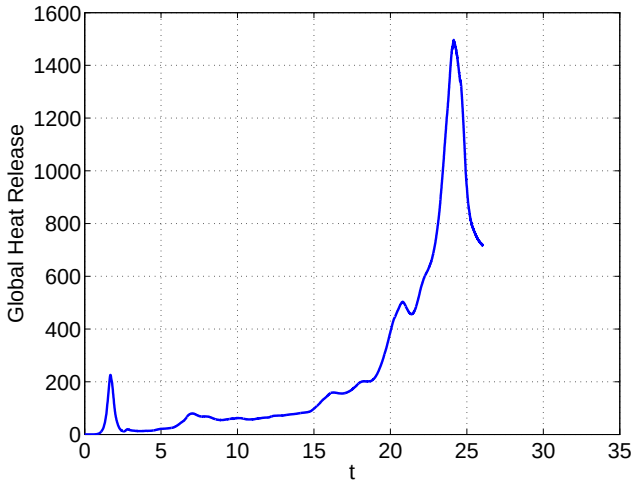

Figure 3. The global heat release rate for two-dimensional detonation initiation ($j_{\max} = 9$) shows several localized maxima occur after the initial power deposition and prior to the global heat release maximum.

V.C.1. Large and Small Scale Comparison

Figure 4 shows a sequence of temperature contours for the $j_{\max} = 7$, 8, and 9 cases. In order to compare the different cases, it is helpful to compare the fine and large scales separately. Since there is no molecular viscosity, and hence no point-wise convergence for the Euler equations, we expect to see a significant difference in the fine scale structures with each increase in resolution. For the large gasdynamic structures, differences are anticipated as well, but our primary interest lies in determining a point at which continued refinement is unnecessary.

Between the three cases for $0 < t < 10$, there is little noticeable difference in the large scale gasdynamic structures such as the lead shock front and location of the burnt-unburnt gas interface. As expected, differences between these two cases exist in the fine scale structures during this initial period. Figure 5 shows contours of temperature and reaction rate plotted with the numerical grid at $t = 7.6$ for the $j_{\max} = 7$ and 9 cases. The interface between the burnt and unburnt gas contains surface fluctuations in the $j_{\max} = 9$ case from both Richtmyer-Meshkov and Kelvin-Helmholtz instabilities. Whereas in the $j_{\max} = 7$ case, these fluctuations have been suppressed. For $t > 10$ the $j_{\max} = 7$ case begins to consume the reactants more quickly than the other two cases and forms a detonation wave in a shorter amount of time.

Up until the last frame, only minor differences in the large scale gasdynamic structures exist between the $j_{\max} = 8$ and $j_{\max} = 9$ cases. The vortical structures near the closed end of the channel show a significant difference on the finer scales. However, it is only between $22 < t < 24$ that there is a notable difference in the large gasdynamic structure characterized by the different detonation formation times. Continued resolution may show larger differences in the fine scale features, but even smaller differences in the large gasdynamic structures.

V.C.2. Global Convergence

As expected, point-wise convergence is not obtainable using the current approach. Thus, it is more illustrative to examine grid dependence using globally integrated quantities, such as the globally integrated heat release defined in Eq. 7.

Figure 6 plots the globally integrated heat release rate for the five different levels of grid resolution $j_{\max} = [5, 6, 7, 8, 9]$. Each curve shows the same general features, such as the initial power deposition peak, explosions in the bottom left and top left corners, and a period of rapid fuel consumption followed by the formation of an over-driven detonation wave. The global maximum indicates a large consumption of fuel in a short period of time and coincides approximately with the formation of the over-driven detonation wave. The time corresponding to the global maximum of the heat release curve will be referred to as the detonation formation time (DFT).

For the low resolution cases, the DFT is shorter than it is for the higher resolution cases. In fact, for the $j_{\max} = 5$ case, the detonation time is approximately half that of the high resolution cases, $j_{\max} = 8$ and 9.

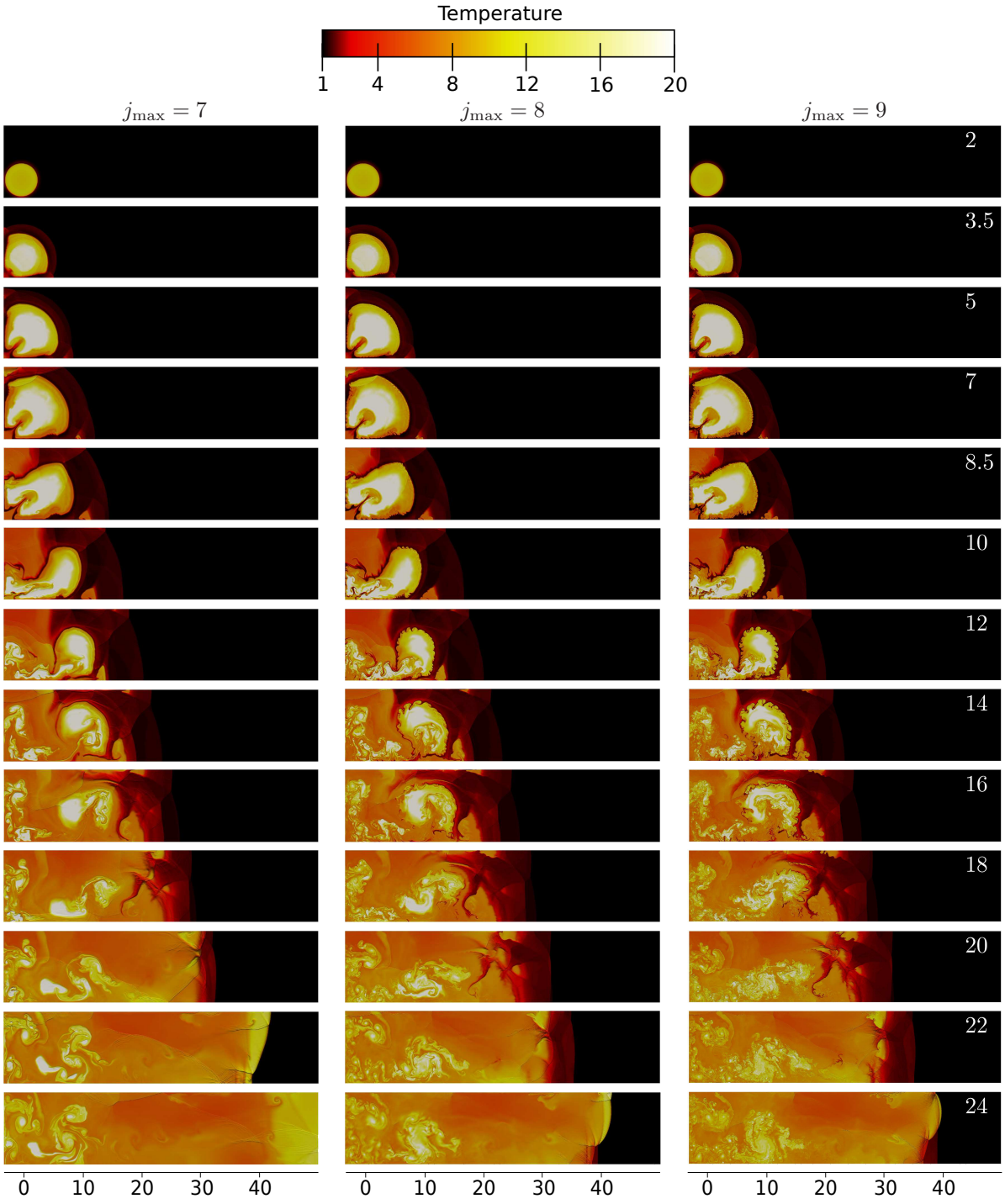

Figure 4. The sequence of temperature contours for $j_{\max} = [7, 8, 9]$ show that while the fine scale structures increase in complexity, the differences in large gasdynamic structures decrease with each increase in resolution.

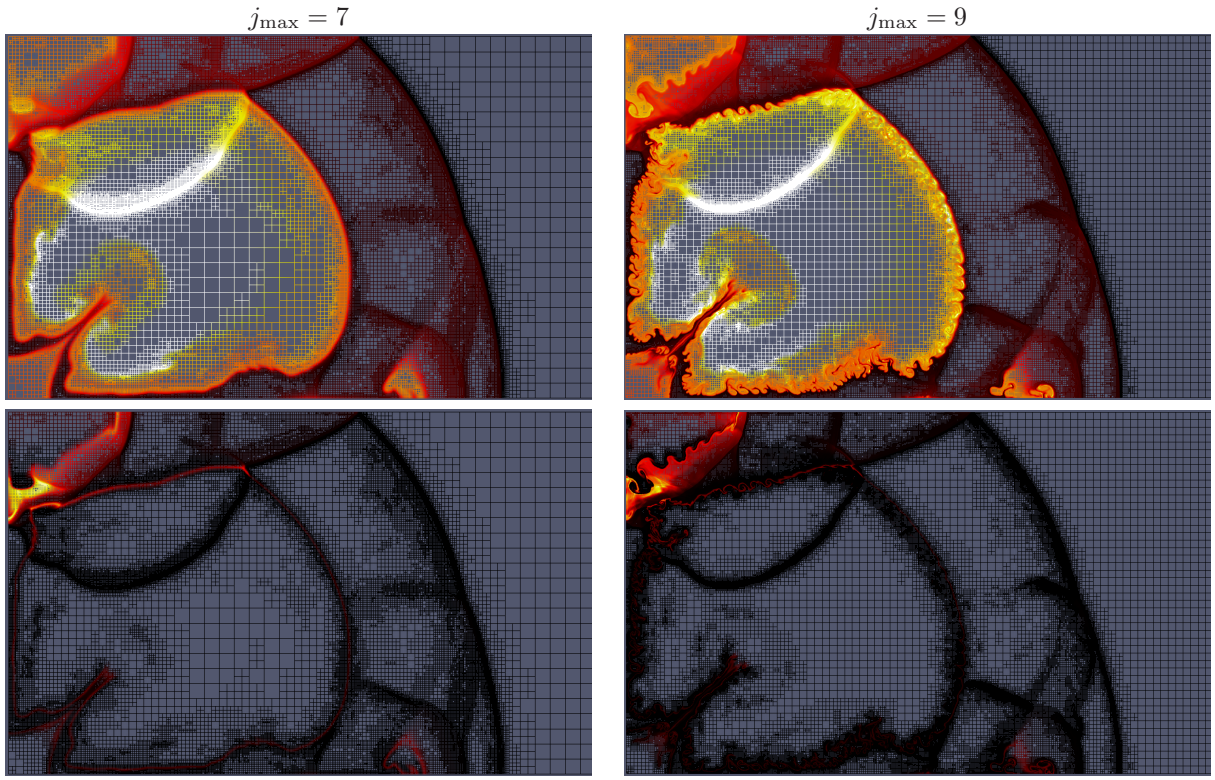

Figure 5. Contour plots for temperature (top) and chemical heat release rate $\dot{W}q$ (bottom) are plotted using a wireframe mesh. The higher resolution case is able to capture surface instabilities from Richtmyer-Meshkov and Kelvin-Helmholtz instabilities, whereas the lower resolution case does not.

The variance between each curve becomes less noticeable as the resolution increases. This indicates that the globally integrated heat release becomes less dependent on the grid spacing as the resolution is increased.

The detonation formation times can be estimated from the global maxima of the heat release in Fig. 6. Since the detonation is not necessarily formed at the peak of the heat release curve, some uncertainty exists in the DFT valuation. Consequently, the width of the peak at half its maximum is used as an uncertainty in obtaining the DFT. Figure 7 plots the DFTs as a function of the minimum grid spacing for each level of resolution on a linear scale. The detonation time increases linearly with decreased grid spacing. This is expected as the numerical algorithm is first order accurate at the burnt-unburnt gas interface as well as shocks.

Figure 7 shows that the difference in detonation formation time between the $j_{\max} = 8$ and 9 cases is within the error of estimation. Extrapolation of the linear curve gives a detonation formation time of $t_0 = 24.7$ for infinite resolution ($\Delta x = 0$). This time can be used as a value for comparison of the DFT error, defined to be $\delta = t - t_0$. Figure 8 plots this error as a function of Δx on a standard log-log scale. It shows that the error is indeed a linear function of the grid spacing.

Figures 7 and 8 show a convergence of the DFT. This indicates a convergence in the larger gasdynamic structures, not a point-wise convergence. An L_∞-norm or other L_x-norms would show that the error actually increases with time. However, since there is no exact solution to compare to, it can be more illustrative to integrate the surface length of the burnt-unburnt gas interface, defined as $Y = 0.5$.

Figure 9 plots the surface length as a function of time for the five different levels of resolution. The surface length is initially identical for each case, but continues to grow at different rates. As expected, the growth rate of the surface length increases with the level of resolution. At some point the growth rate is reduced until the surface length reaches a maximum. Subsequently the surface length decreases until it reaches a value of approximately 12, which corresponds to the surface length of the detonation wave. The surface length reaches its final value at roughly the same time (approximately $t = 25$) for the $j_{\max} = 8$ and 9 cases. This is a slightly later time than that observed from the peak heat release times observed in Fig. 6.

It is clear from Fig. 9 that there is indeed no point-wise convergence. It is also evident that a larger global

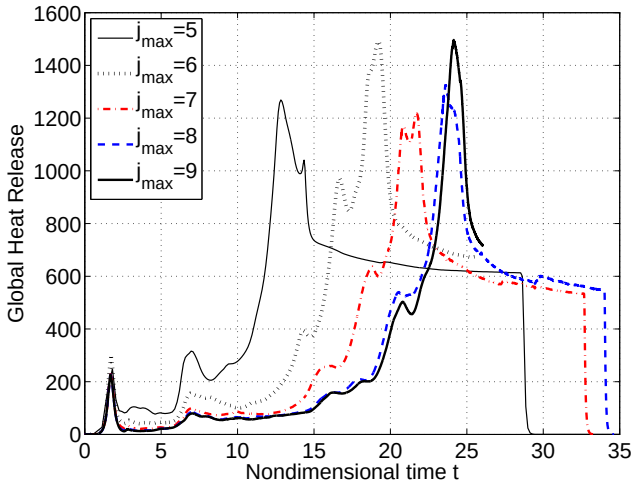

Figure 6. Heat release profiles for the 5 different levels of resolution. The differences between each successive profile diminish with increasing resolution.

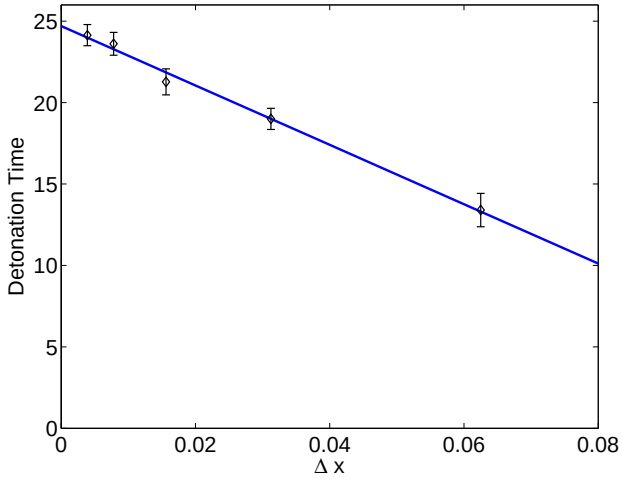

Figure 7. The convergence rate for two-dimensional detonation initiation is linear. The extrapolation line indicates that finer resolution will increase the peak heat release time by less than 5%.

scale does exist, that is independent of the fine-scale structures, that is temporally resolved with increasing grid resolution.

V.C.3. Competition Between Scales

The growth, peak, and reduction of the surface length suggests a competition between large and small scales exists. The scale associated with the reduction of the surface length is dictated by the chemical reaction and is dependent upon geometry and power deposition parameters. As expected, without molecular diffusion/viscosity, the size of the small scale structures is governed implicitly through the numerical algorithm.

At $j_{\max} = 8$ and 9, the differences in the large gasdynamic structures become small enough that the detonation formation times are nearly equal for the two cases. This shift from a strong dependence on grid resolution for cases with $j_{\max} \leq 7$ to a regime where the DFT is relatively independent of resolution for cases $j_{\max} > 7$ marks a transition in behavior. In order to understand how this shift in behavior occurs, it is helpful to compare fuel density contours for the $j_{\max} = 7$ and 9 cases. The fuel density is used instead of density or temperature, because what occurs inside the reacted fluid does not bear much influence on the changes in behavior and it makes the differences more apparent.

Figure 10 shows a sequence of contours of the fuel density for the $j_{\max} = 7$ and 9 cases for $t = [5, 6, 7, 8]$. The initial power deposition created the explosion at $t = 2$ and the small explosion in the bottom left corner occurred at $t = 2.5$. The lead shock front is just about to reflect off the upper wall and create a localized

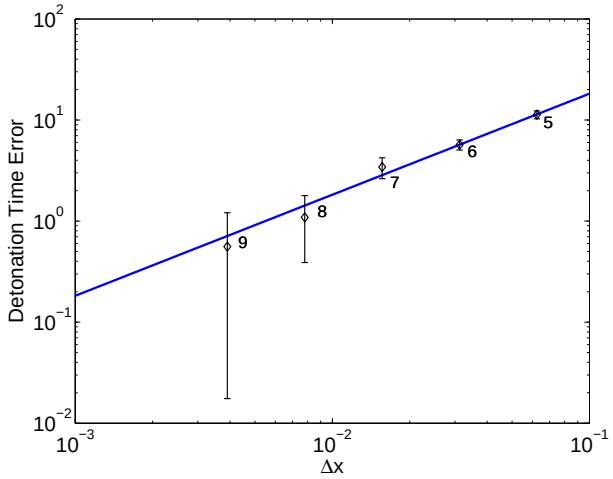

Figure 8. The error between the extrapolated detonation time and the detonation time at a given grid resolution shows a linear dependence on grid spacing.

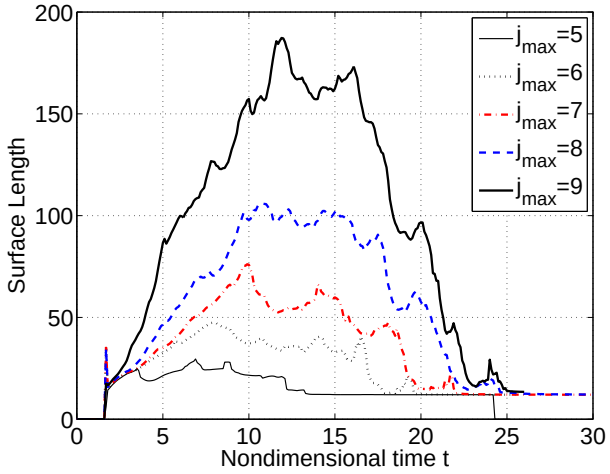

Figure 9. As indicated by the increase in slopes for increasing resolution, at early times the growth rate of the total surface length L_s increases with resolution. The independence of the DDT time from grid resolution is demonstrated by the surface length converging to the DDT surface length for both $j_{\max} = 8$ and $j_{\max} = 9$.

explosion.

Comparison of the $t = 5$ contours indicate that the Richtmyer-Meshkov instabilities that occur at the burnt-unburnt gas interface are better resolved in the $j_{\max} = 9$ case. The typical mushroom shape of an RM instability is present in the $j_{\max} = 9$ case. Whereas in the $j_{\max} = 7$ case, numerical diffusion has preheated the reactants near the end of the mushroom tip, causing them to be consumed in a chemical reaction leaving behind only part of the instability seen in the $j_{\max} = 9$ case.

In each of the four time instances, the available fuel located in the bottom left corner is consumed more rapidly in the lower resolution case. It can be seen that only a very small portion of the fuel in the bottom corner was consumed in the initial explosion at $t = 2.5$. The rest of the fuel is consumed over a longer period of time. By $t = 8$, more fuel has been consumed in the $j_{\max} = 7$ case than in the $j_{\max} = 9$ case. In the $j_{\max} = 9$ case, RM instabilities combined with a reduction in numerical diffusion have allowed more reactants to persist inside of this volatile region before being consumed by the chemical reaction. In the lower resolution case these instabilities are suppressed by the numerical diffusion, which causes the more rapid consumption of the fuel in this region.

The explosion in the upper left corner can be seen in the last two time instances of Fig. 10 for $t = 7$ and 8. At $t = 7$, there is little difference in fuel consumption between the two cases. A moment later at $t = 8$, Richtmyer-Meshkov instabilities are clearly visible in the $j_{\max} = 9$ case. Whereas in the $j_{\max} = 7$ case, these

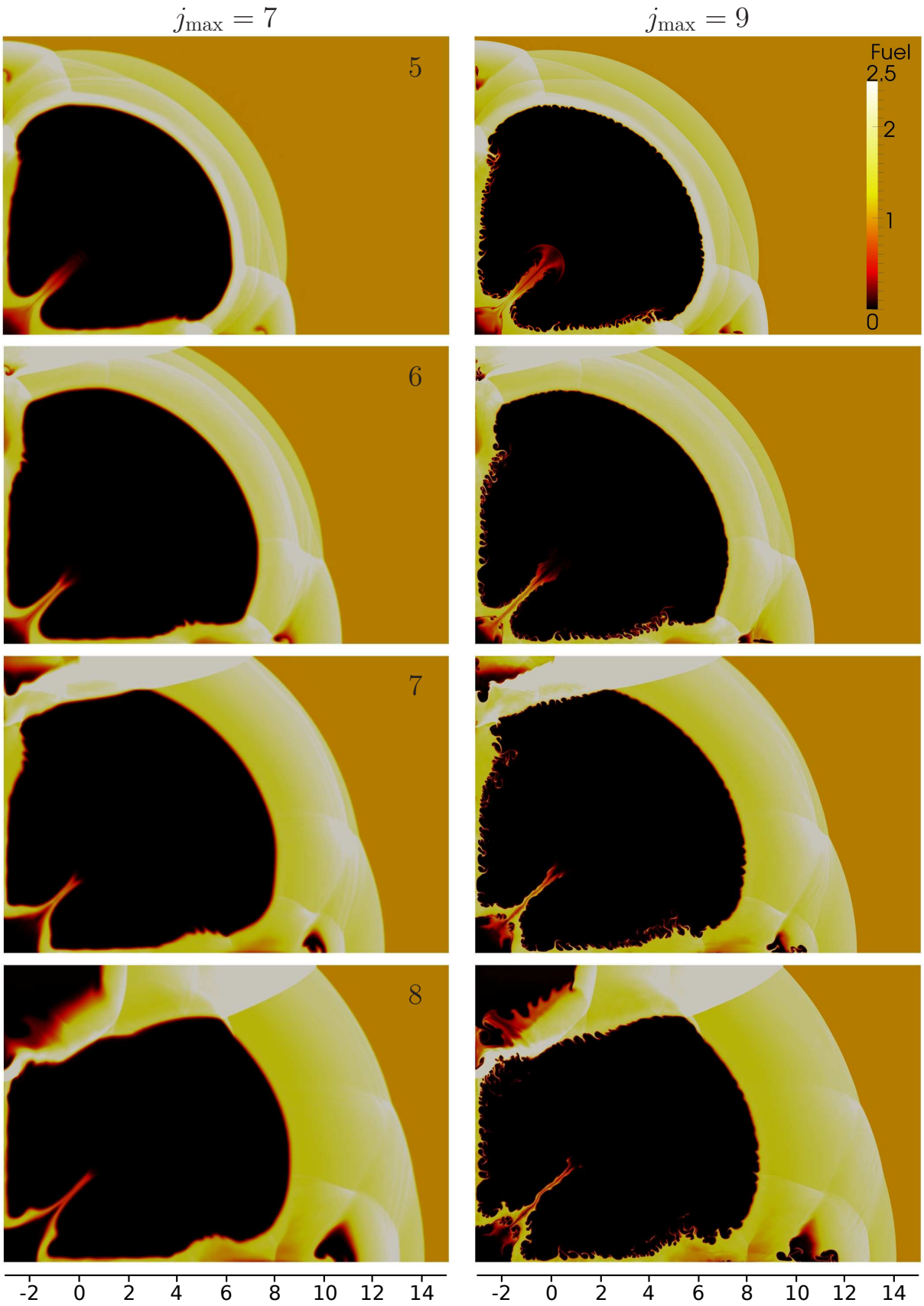

Figure 10. Sequence of contours for fuel density ρY at $j_{\max} = 7$ and $j_{\max} = 9$ show that overall the large scale gasdynamic structures are very similar with only minor differences at the burnt-unburnt gas interface ($t = 5, 6, 7, 8$).

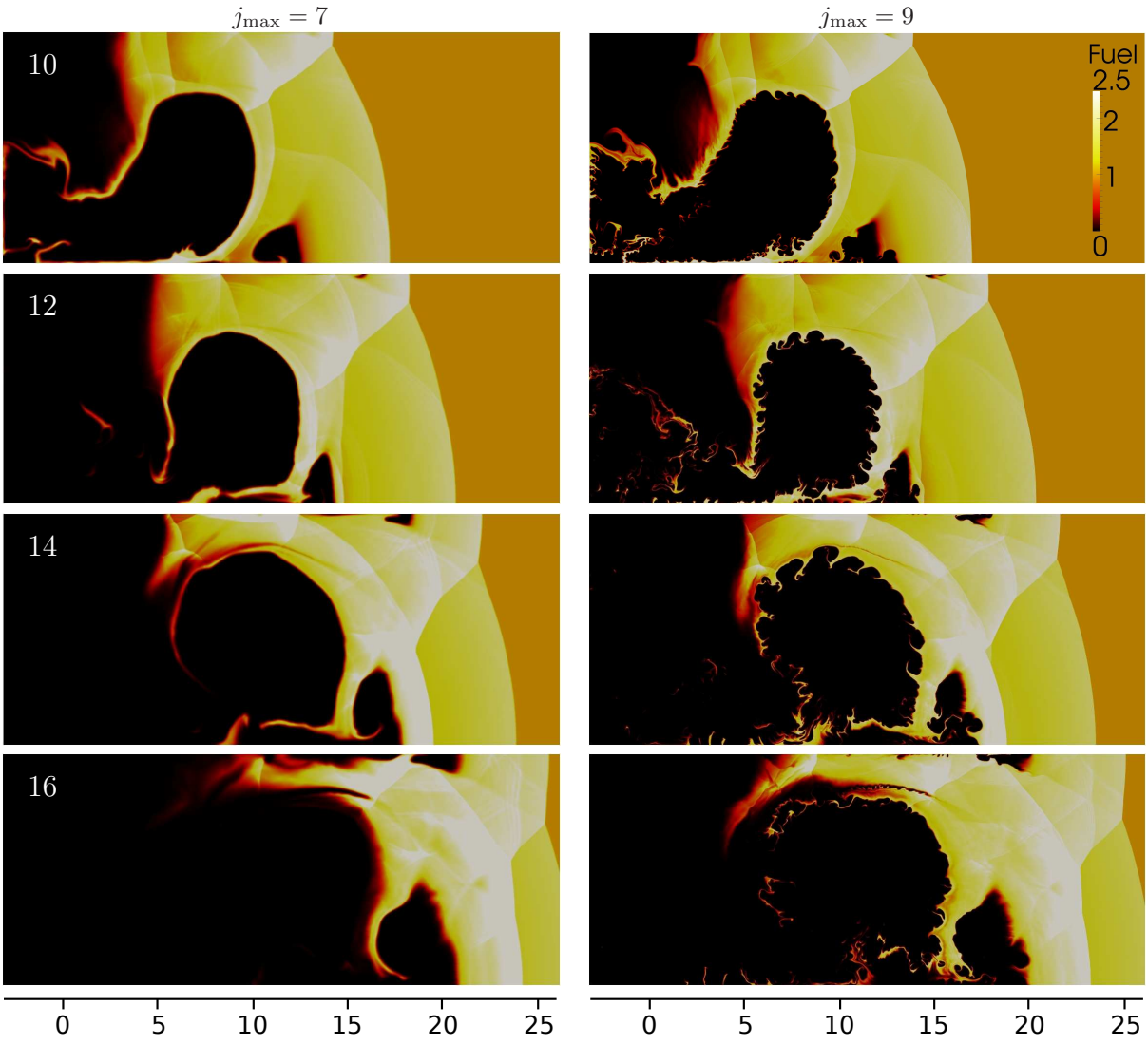

Figure 11. Sequence of contours for fuel density ρY at $j_{\max} = 7$ and $j_{\max} = 9$ show that overall the large scale gasdynamic structures are similar in the beginning, but the lower resolution case consumes the reactants at a faster rate and by $t = 16$, significant differences exist ($t = 10, 12, 14, 16$).

instabilities are suppressed by numerical diffusion/viscosity.

At $t = 10$, little difference can be observed between the two cases in the globally integrated heat release in Fig. 6. Between $10 \leq t \leq 16$, there is a substantial deviation in heat release between the two cases. The $j_{\max} = 7$ case consumes fuel more rapidly, ultimately leading to an earlier detonation formation time.

Figure 11 shows the fuel density contours for the $j_{\max} = 7$ and 9 cases at $t = [10, 12, 14, 16]$. Both cases show the presence of unreacted fuel pockets inside the burnt region and are qualitatively very similar. However, the lower resolution case shows a more diffuse interface from higher levels of numerical diffusion. As time commences, the unreacted fuel pockets are consumed, but the pockets in the $j_{\max} = 9$ case are consumed more slowly and are allowed to stretch and fold without being immediately diffused. By $t = 16$, it is visible that the $j_{\max} = 7$ case has consumed more reactants than the $j_{\max} = 9$ case. This is consistent with the deviation in heat release rate observed in Fig. 6. The numerical diffusion is transferring heat more rapidly to the reactive fluid, which facilitates a more rapid detonation formation.

Figure 6 shows that there are only minor differences in heat release between the $j_{\max} = 8$ and 9 cases. This suggests that between these two cases, the unreacted pockets are consumed at approximately the same rate. In other words, a scale has been resolved (or is at least close to being resolved). The resolved scale is the diffusionless ignition delay time of the unreacted pockets.[2] Each unreacted fluid volume has an autoignition

time. If the resolution is increased to a point where the numerical diffusion becomes so small that the timescale associated with fuel pocket consumption is long compared to the diffusionless ignition delay time, unreacted fuel pockets will react in a "purely gasdynamic" manner.

Once high enough resolution is achieved, surface instabilities are able to entrain unreacted fluid into reacted regions. If the entrained fluid is able to persist as unreacted pockets of fluid inside the reacted fluid such that the pocket's consumption rate is governed by the gasdynamic processes and not diffusional processes, the detonation formation time will become insensitive to the grid resolution and numerical diffusion/viscosity. It is this criteria that allows the DFT to converge while being independent of the level of resolution. This suggests that the indirect detonation initiation process presented in the $j_{\max} = 8$ and 9 cases can be considered "purely gasdynamic".

VI. Discussion

The detonation formation time is shown to be strongly dependent upon grid resolution for $j_{\max} \leq 7$. Numerical diffusion, implicitly present in virtually all hyperbolic flow solvers, artificially diffuses shocks and material interfaces. This is consistent with previous observations that show that with insufficient resolution, the numerical diffusion can be just as diffusive, if not more diffusive than the molecular diffusion.[24,25]

As resolution is increased for $j_{\max} \geq 8$, the detonation formation time becomes relatively independent of numerical resolution. However, it is clear that there is no point-wise convergence that occurs. As resolution increases, the surface length of the material interface grows more rapidly with higher resolution. The contour plots for the cases $j_{\max} = 8$ and 9 show the generation of both Richtmyer-Meshkov and Kelvin-Helmholtz instabilities. As demonstrated in Ref. 1 and 18, Richtmyer-Meshkov instabilities are the primary driver of flow instability and are present even in the highly under-resolved cases $j_{\max} \leq 7$. However, in these under-resolved simulations, the unreacted pockets of fluid entrained into the reacted products are quickly consumed due to a high level of numerical diffusion. In the higher resolution cases, the numerical resolution is reduced such that Kelvin-Helmholtz instabilities, which have been shown to be suppressed in DDT Navier-Stokes simulations,[1,18] are able to exist and interact with Richtmyer-Meshkov instabilities to entrain unreacted fluid into regions of reacted products.

The existence of Kelvin-Helmholtz instabilities suggests that the numerical diffusion may be playing a minor role in the heating and subsequent consumption of the unreacted pockets. This makes the detonation formation process become independent of the fine scale structures and only dependent upon the large gasdynamic heating mechanisms. Convergence of the detonation formation time, irrespective of the fact that there is no point-wise convergence, implies that a scale is being resolved. This scale is the diffusionless ignition delay time of the unreacted pockets[2] that are formed from the instabilities at the burnt-unburnt gas interface. Each unreacted pocket has been preheated such that it will ignite after some predetermined time without the diffusion of heat from the surrounding reacted products. The dimensional activation energy for the cases in the current work is approximately $E' = 11.5\,\text{kcal/mol}$. The current results are analogous to that seen in Ref. 2 and 4 where the diffusionless ignition delay time of unreacted pockets was resolved.

VII. Conclusions

Two-dimensional simulations using the reactive Euler equations deposit energy in a cylindrical volume of fluid during a finite time on the order of the acoustic timescale of the heating volume. The simulations demonstrate that numerical diffusion strongly influences the detonation formation time. The results also suggest that given sufficient resolution, it is possible to achieve "purely gasdynamic" indirect detonation initiation, where the formation process is virtually independent of diffusion. This claim is validated by demonstrating that the detonation formation times obtained from both the peak heat release and surface length plots converge with increased resolution. As the resolution increases, Richtmyer-Meshkov and Kelvin-Helmholtz instabilities entrain unreacted pockets of reactive fluid inside regions of reacted products. The longevity that these pockets exist inside the reacted region is attributed to the minimal amounts of artificial diffusion imposed at the pocket interface. This allows the diffusionless ignition delay time of the pocket to be resolved, which results in a detonation formation time that is independent of grid resolution.

The ability to achieve "purely gasdynamic" indirect detonation initiation may be useful because it indicates that a particular configuration is detonable for all diffusivities. This essentially provides a mechanism for determining an upper bound on the energy and power constraints required in order to detonate a reactive

mixture. Although these results are compelling, the current work is limited to two dimensions. Further work is required to determine if the conclusions made in this work can be extended to three dimensions.

VIII. Acknowledgements

J.D.R. would like to thank Guillaume Blanquart for the use of his computational resoures in performing the simulations contained in this work.

References

[1]Oran, E. S. and Gamezo, V. N., "Origins of the deflagration-to-detonation transition in gas-phase combustion," *Combustion and Flame*, Vol. 148, No. 1-2, Jan. 2007, pp. 4–47.

[2]Radulescu, M. I., Sharpe, G. J., Law, C. K., and Lee, J. H. S., "The hydrodynamic structure of unstable cellular detonations," *Journal of Fluid Mechanics*, Vol. 580, May 2007, pp. 31.

[3]Dorofeev, S. B., "Flame acceleration and explosion safety applications," *Proceedings of the Combustion Institute*, Vol. 33, No. 2, Jan. 2011, pp. 2161–2175.

[4]Mazaheri, K., Mahmoudi, Y., and Radulescu, M. I., "Diffusion and hydrodynamic instabilities in gaseous detonations," *Combustion and Flame*, Vol. 159, No. 6, June 2012, pp. 2138–2154.

[5]Romick, C. M., Aslam, T. D., and Powers, J. M., "The effect of diffusion on the dynamics of unsteady detonations," *Journal of Fluid Mechanics*, Vol. 699, April 2012, pp. 453–464.

[6]Kassoy, D. R., "The response of a compressible gas to extremely rapid transient, spatially resolved energy addition: an asymptotic formulation," *Journal of Engineering Mathematics*, Vol. 68, No. 3-4, Aug. 2010, pp. 249–262.

[7]Oppenheim, A. K. and Urtiew, P. A., "Experimental observations of the transition to detonation in an explosive gas," *Proc. Roy. Soc. A*, Vol. 295, 1966, pp. 13–28.

[8]Clarke, J. F., Kassoy, D. R., and Riley, N., "On the direct initiation of a plane detonation wave," *Proc. Roy. Soc. London A.*, Vol. 408, 1986, pp. 129–148.

[9]Clarke, J. F., Kassoy, D. R., Meharzi, N. E., Riley, N., and Vasantha, R., "On the Evolution of Plane Detonations," *Proc. Roy. Soc. London A.*, Vol. 429, No. 1877, 1990, pp. 259–283.

[10]Kassoy, D. R., Kuehn, J. A., Nabity, M. W., and Clarke, J. F., "Detonation initiation on the microsecond time scale: DDTs," *Combustion Theory and Modelling*, Vol. 12, No. 6, Nov. 2008, pp. 1009–1047.

[11]Regele, J. D., Kassoy, D. R., and Vasilyev, O. V., "Effects of high activation energies on acoustic timescale detonation initiation," *Combustion Theory and Modelling*, , No. January, Jan. 2012, pp. 1–29.

[12]Khokhlov, A. M. and Oran, E. S., "Numerical simulation of detonation initiation in a flame brush: the role of hot spots," *Combustion and Flame*, Vol. 119, No. 4, Dec. 1999, pp. 400–416.

[13]Khokhlov, A., Oran, E., and Thomas, G., "Numerical simulation of deflagration-to-detonation transition: the role of shock–flame interactions in turbulent flames," *Combustion and Flame*, Vol. 117, No. 1-2, April 1999, pp. 323–339.

[14]Oran, E. S. and Khokhlov, A. M., "Deflagrations, hot spots, and the transition to detonation," *Philosophical Transactions of the Royal Society A: Mathematical, Physical and Engineering Sciences*, Vol. 357, No. 1764, Dec. 1999, pp. 3539–3551.

[15]Gamezo, V. N., Khokhlov, A. M., and Oran, E. S., "The influence of shock bifurcations on shock-flame interactions and DDT," *Combustion and Flame*, Vol. 126, No. 4, Sept. 2001, pp. 1810–1826.

[16]Kessler, D. A., Gamezo, V. N., and Oran, E. S., "Simulations of flame acceleration and deflagration-to-detonation transitions in methane–air systems," *Combustion and Flame*, Vol. 157, No. 11, Nov. 2010, pp. 2063–2077.

[17]Ivanov, M., a. Kiverin, and Liberman, M., "Hydrogen-oxygen flame acceleration and transition to detonation in channels with no-slip walls for a detailed chemical reaction model," *Physical Review E*, Vol. 83, No. 5, May 2011, pp. 1–16.

[18]Gamezo, V. N., Desbordes, D., and Oran, E. S., "Formation and evolution of two-dimensional cellular detonations," *Combustion and Flame*, Vol. 116, No. 1-2, Jan. 1999, pp. 154–165.

[19]Oran, E. S., Weber Jr., J. W., Stefaniw, E. I., Lefebvre, M. H., and Anderson Jr., J. D., "A Numerical Study of a Two-Dimensional H2-O2-Ar Detonation Using a Detailed Chemical Reaction Model," *Combustion and Flame*, Vol. 113, 1998, pp. 147–163.

[20]Vasilyev, O. V. and Bowman, C., "Second-Generation Wavelet Collocation Method for the Solution of Partial Differential Equations," *Journal of Computational Physics*, Vol. 165, No. 2, Dec. 2000, pp. 660–693.

[21]Kevlahan, N. K. R. and Vasilyev, O. V., "An adaptive wavelet collocation method for fluid-structure interaction at high reynolds numbers," *Sciam J Sci Comput*, Vol. 26, No. 6, 2005, pp. 1894–1915.

[22]Regele, J. D. and Vasilyev, O. V., "An adaptive wavelet-collocation method for shock computations," *International Journal of Computational Fluid Dynamics*, Vol. 23, No. 7, Aug. 2009, pp. 503–518.

[23]Regele, J. D., *Numerical modeling of acoustic timescale detonation initation using the adaptive wavelet-collocation method*, Ph.d. thesis, University of Colorado, Boulder, Feb. 2008.

[24]Singh, S., Powers, J. M., and Paolucci, S., "Detonation Solutions from Reactive Navier-Stokes Equations," *37th AIAA Aersopace Sciences Meeting and Exhibit*, Vol. AIAA-99-09, 1999.

[25]Sharpe, G. J., "Transverse waves in numerical simulations of cellular detonations," *Journal of Fluid Mechanics*, Vol. 447, Oct. 2001, pp. 31–51.